Effects of curvature on rarefied gas flows between rotating concentric cylinders

PHYSICS OF FLUIDS **25**, 052003 (2013)

Effects of curvature on rarefied gas flows between rotating concentric cylinders

Nishanth Dongari,[a] Craig White,[b] Thomas J. Scanlon,[c] Yonghao Zhang,[d] and Jason M. Reese[e]
James Weir Fluids Lab, Department of Mechanical & Aerospace Engineering, University of Strathclyde, Glasgow G1 1XJ, United Kingdom

(Received 26 November 2012; accepted 22 April 2013; published online 23 May 2013)

The gas flow between two concentric rotating cylinders is considered in order to investigate non-equilibrium effects associated with the Knudsen layers over curved surfaces. We investigate the nonlinear flow physics in the near-wall regions using a new power-law (PL) wall-scaling approach. This PL model incorporates Knudsen layer effects in near-wall regions by taking into account the boundary limiting effects on the molecular free paths. We also report new direct simulation Monte Carlo results covering a wide range of Knudsen numbers and accommodation coefficients, and for various outer-to-inner cylinder radius ratios. Our simulation data are compared with both the classical slip flow theory and the PL model, and we find that non-equilibrium effects are not only dependent on Knudsen number and accommodation coefficient but are also significantly affected by the surface curvature. The relative merits and limitations of both theoretical models are explored with respect to rarefaction and curvature effects. The PL model is able to capture some of the nonlinear trends associated with Knudsen layers up to the early transition flow regime. The present study also illuminates the limitations of classical slip flow theory even in the early slip flow regime for higher curvature test cases, although the model does exhibit good agreement throughout the slip flow regime for lower curvature cases. Torque and velocity profile comparisons also convey that a good prediction of integral flow properties does not necessarily guarantee the accuracy of the theoretical model used, and it is important to demonstrate that field variables are also predicted satisfactorily.
 [http://dx.doi.org/10.1063/1.4807072]

I. INTRODUCTION

Isothermal gas flow between two concentric rotating cylinders is a classical fluid dynamics problem that is detailed for the no-slip case in many well-known textbooks (e.g., Schlichting[1]). However, under certain rarefied conditions the flow between the cylinders can exhibit highly non-intuitive behaviour. For example, if the outer cylinder is stationary and the inner cylinder is rotating, it is possible for the velocity profile to become *inverted*, i.e., the velocity will *increase* from the inner to the outer cylinder wall. This unusual flow phenomenon was first described theoretically by Einzel *et al.*[2] for the case of liquid helium. Using the direct simulation Monte Carlo (DSMC) technique, Tibbs *et al.*[3] extended the analysis to the case of a rarefied gas and demonstrated that velocity inversion could occur provided the tangential momentum accommodation coefficient (TMAC) for the surfaces was small. This early work has led to a number of theoretical and simulation studies for rotating Couette flow[4–12] and oscillating Couette flow.[13] These confirmed the existence of velocity inversion

[a]Electronic mail: nishanth.dongari@strath.ac.uk
[b]Electronic mail: craig.white@strath.ac.uk
[c]Electronic mail: tom.scanlon@strath.ac.uk
[d]Electronic mail: yonghao.zhang@strath.ac.uk
[e]Electronic mail: jason.reese@strath.ac.uk

for small values of TMAC and also showed there was a critical accommodation coefficient.[14,15] Indeed, Yuhong *et al.*[5] derived an analytical criterion for the critical accommodation coefficient and showed that velocity inversion was solely dependent on the value of TMAC at the stationary outer cylinder.

Yuhong *et al.*[5] also discussed the limitations of classical slip flow theories: they are only applicable up to $Kn \sim 0.1$. This has generally led to second-order treatments of the velocity slip at solid bounding surfaces,[16] but with limited success because this approach fails to reproduce the nonlinear stress/strain-rate relationship observed in the Knudsen layer (KL).[10,17–19] The behaviour of a rarefied gas in the Knudsen layer can accurately be predicted by the Boltzmann equation.[20,21] However, directly solving the Boltzmann equation for practical gas flow applications remains computationally intensive due to the complicated structure of the molecular collision term. Other alternatives are to introduce a slip coefficient that depends on the Knudsen number[22] or to introduce an effective viscosity term.[23,24] Cercignani used kinetic theory to propose a "wall-function" that scales with the mean free path.[20] This function complements the constitutive relation by effectively modifying the viscosity, and is able to capture some non-equilibrium behaviour of the Knudsen layer. This idea has been adopted and extended[16,25–28] with some success.

Dongari *et al.*[29] carried out molecular dynamics (MD) simulations of gases and the results indicate that molecules perform Lévy-type flights[30] under rarefied conditions, i.e., the free paths of gas molecules follow a power-law (PL) distribution. Consequently, these authors hypothesised that the probability distribution function for the molecular free paths of a rarefied gas followed a PL form, and this was validated against MD data under various rarefied conditions. Using a PL distribution to describe free paths, Dongari *et al.*[31] and Dongari *et al.*[32] derived effective mean free path (MFP) models for flows confined by planar and non-planar surfaces, respectively, by taking into account the solid boundary effects. PL effective MFP models showed good agreement with the MD data up to the early transition regime ($Kn \sim 1$), while classical exponential MFP scaling models[33,34] are limited up to $Kn \sim 0.2$. In addition, these authors modified the Navier-Stokes constitutive relations and slip boundary conditions using PL-based MFP scaling and were then able to accurately capture several non-equilibrium effects in the Knudsen layer for both isothermal and thermal gas flows.

On the other hand, particle simulation methods such as DSMC[35] and MD[36] not only provide excellent alternatives to solve rarefied gas flows, but also aid in rigorously validating these kinds of extended hydrodynamic models. Existing simulations for cylindrical Couette flows[3,37] do not cover a wide range of Knudsen numbers, and they are only carried out for limited ratios of radii of the outer (R_2) to inner (R_1) cylinders. Tibbs *et al.*[3] presented DSMC results for $Kn = 0.5$, with $R_2/R_1 = 5/3$, while Kim's[37] MD numerical experiments are conducted for $Kn \simeq 0.01$, with $R_2/R_1 = 5$. Although Jung[38] has performed MD simulations for various radii ratios, the R_2/R_1 values in this work are quite large ($\gg 5$) and the rotating inner cylinder may have lesser influence on the velocity profile results.

There is also a scarcity of torque data for the rotating Couette flow test case. The existing experimental data can be traced back to Kuhlthau,[39] however, these experiments were performed for a set-up where the length of the inner cylinder is comparable to its radius. It has been mentioned by Agrawal and Prabhu,[14] that one needs to incorporate a correction factor to match the classical theories in the continuum regime.

In view of the above, we carry out rigorous DSMC simulations of cylindrical Couette gas flow for Knudsen numbers covering the slip ($Kn = 0.1$) and transition flow regime ($Kn = 0.5$ and 1). At each Kn, a variety of TMAC (σ) and R_2/R_1 values are used to check the sensitivity of surface and curvature effects, respectively. The resultant velocity and torque data are compared with the classical slip theory and the new PL wall scaling model.[31,32] A brief overview of our DSMC simulations and the PL wall-scaling model are outlined in Secs. II–IV.

II. DSMC SIMULATIONS

We investigate gas flows in the transition flow regime, so the DSMC method[35] is chosen to provide our numerical results. DSMC is a stochastic particle-based method, in which a single DSMC simulator particle can represent any number of real gas molecules, and particle movements

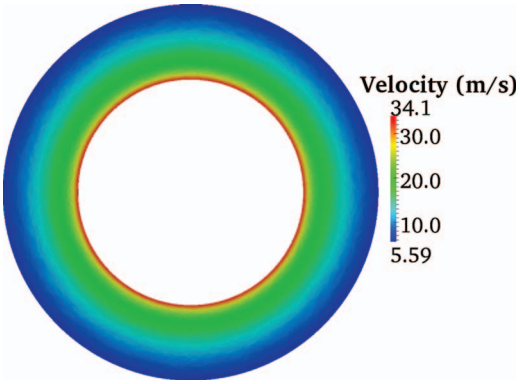

FIG. 1. Contours of velocity calculated by *dsmcFoam* for a typical concentric cylindrical Couette flow case.

and collisions are decoupled. Particle movements are handled deterministically according to the particle velocity vectors and the simulation time step. Binary inter-molecular collisions and surface interactions are dealt with in a probabilistic manner. Macroscopic properties are recovered as a spatial and time average of the microscopic particle properties.

The DSMC solver used in this paper is *dsmcFoam*, an open source solver that is part of the free-to-download C++ fluid dynamics toolbox, OpenFOAM.[40] This solver has previously been rigorously validated for a variety of benchmark cases.[41,42] Two-dimensional DSMC simulations of cylindrical Couette flows are reported in the present paper, where argon gas is trapped between two concentric cylinders. The inner cylinder is rotating and the outer cylinder is stationary. Our simulations do not utilise quarter or half symmetry: a full circular domain is modelled as shown in Figure 1.

As validation for *dsmcFoam* for rarefied, low-speed cylindrical Couette flow, results are compared to previous DSMC results for the transition regime with hard sphere STP argon as the working gas.[3] The inner cylinder has a radius R_1 of 1.875×10^{-7} m and the outer cylinder's radius R_2 is 3.125×10^{-7} m, which gives $R_2/R_1 = 5/3$. The Knudsen number based on the hard sphere mean free path λ (6.33×10^{-8} m) and the gap between the two cylinders is 0.5. The inner cylinder rotates with a constant velocity of 96.94 m/s, giving a Mach number of 0.3. Excellent agreement with previous

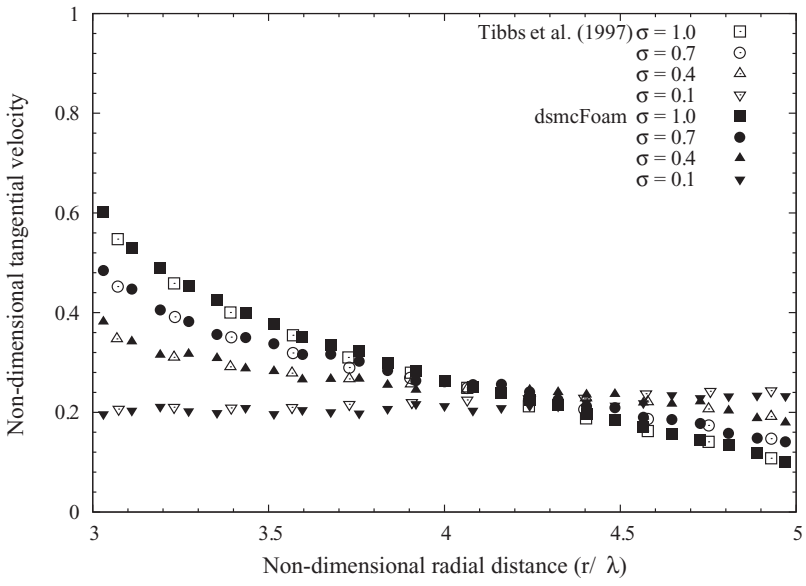

FIG. 2. Comparison of DSMC tangential velocity profiles from *dsmcFoam* and Ref. 3.

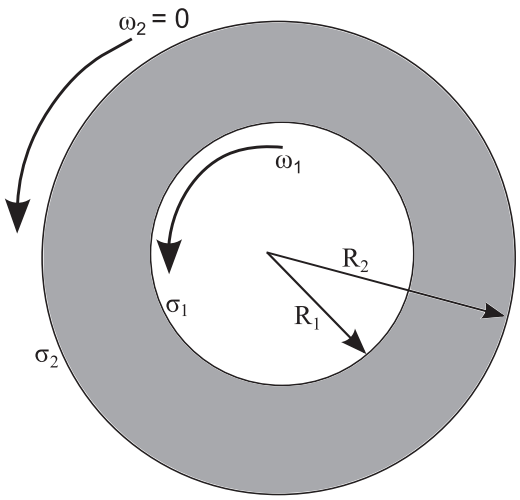

FIG. 3. Schematic of Couette flow between concentric rotating cylinders.

results for the normalised velocity profiles with four different accommodation coefficients (1.0, 0.7, 0.4, and 0.1) can be observed in Figure 2.

For all of the remaining DSMC simulations reported in this paper, the numerical cell size is chosen such that the cells are much smaller than the mean free path, and so that enough cells are placed throughout the domain to recover macroscopic properties with sufficient resolution. The Knudsen number is based on the ratio of the unconfined mean free path value (λ) to the radial distance between the cylinder surfaces ($R_2 - R_1$). The time step is smaller than the mean collision time, and also small enough that particles are likely to spend multiple time steps within a single computational cell. All simulations are initialised with at least 20 DSMC particles per cell, and 500 000 particles in the whole domain. Each case was solved in parallel on 4 cores of the 1100 core High Performance Computer (HPC) facility at the University of Strathclyde. The run time for each case was around 60 h to achieve a total of at least 300 000 samples. The variable hard sphere collision model[43] is used to perform collisions, and all surface-particle interactions are dealt with as a mixture of specular and diffuse interactions in order to simulate various accommodation coefficients. The torque on the rotating inner cylinder is calculated from the measured viscous drag force acting on the inner cylinder surface.

Numerical results are obtained for a variety of outer-to-inner cylinder radius ratios (R_2/R_1 = 6/5, 5/3, 2, 3, and 5), Knudsen numbers (0.1, 0.5, and 1.0) and accommodation coefficients (0.1, 0.4, 0.7, and 1.0), as shown in Figure 3. The inner cylinder is rotating at a Mach number ($Ma = R_1\omega/\sqrt{\gamma RT}$) of 0.20 for all simulated test cases. Here ω is the angular velocity of the inner cylinder, γ the ratio of the specific heat capacities, R the gas constant, and T the temperature. The surface temperature of both cylinders is constant at 273 K. The radii ratio is varied by fixing R_1 and increasing R_2, and Kn is maintained constant by proportionally modifying the gas density. As the Mach number is fixed, the Reynolds number ($Re = Ma/Kn\sqrt{\pi\gamma/2}$) remains constant for different geometric configurations, as long as Kn is constant.

III. POWER-LAW WALL SCALING MODEL

Close to a solid boundary, gas molecule-surface interactions start to dominate gas inter-molecular collisions. Hence, the gas MFP will effectively be reduced in the near-wall regions, leading to a nonlinear variation of MFP with surface normal distance.[33] This leads to the formation of a KL: a local thermodynamically non-equilibrium region extending $\sim O(\lambda)$ from the surface.[21] The state of non-equilibrium induced by a surface should be spatially extended in proportion to the probability of a collisionless trace of molecule travelling a certain distance from a wall. Therefore, by investigating the variation of the effective MFP a more accurate indication of the KL extent can be obtained.

Dongari *et al.*[32,44] derived a PL-based effective MFP model for non-planar surfaces by incorporating the effects of curvature. They developed a curvature-dependent MFP solution for both convex and concave surfaces, and extended this analysis to deduce the effective MFP for a gas confined between two concentric cylinders. In the present paper, we incorporate this power-law wall scaling model developed for cylindrical surfaces into the Navier-Stokes equations. The non-planar MFP solution reduces to the planar wall MFP model[31] when the curvature tends to zero and the non-planar solution also satisfies other limiting conditions.[32]

The current setup has gas confined between two co-axial cylinders. In this context, the curvature effects are induced due to both the convex (inner cylinder) and the concave (outer cylinder) nature of the surfaces, and it is very important to capture this nonlinear behaviour accurately. For example, in the case of planar parallel walls, it is equally probable that a molecule travels towards one surface or the other.[31] However, in the present case solid angle theory is used to determine the likelihood of a molecule travelling in the direction of cylinder, as opposed to travelling towards the bulk or other cylinder. From this weighting, the general expression for the effective mean free path of a gas is obtained.[32] The convex surface (inner cylinder) overpredicts gas MFP compared to a planar case, while the concave surface (outer cylinder) underpredicts it. This stems from the fact that gas molecules near a convex surface have more probability to travel towards the bulk, while they have smaller probability near a concave surface.[32] The differences between these over- and underpredictions are magnified with increase in R_2/R_1. So the curvature effects are very important for the current power-law model and used to modify the Navier-Stokes equations to explore the nonlinear physics associated with the Knudsen layers of rarefied gas flows confined between rotating co-axial cylinders.

A. Effective mean free path

The complete expression for the normalised (by the conventional unconfined MFP) effective mean free path of a gas confined between two concentric cylinders is[32,44]

$$\beta = \left(\frac{\theta_u^-}{\pi}\right)\left[1 - \frac{1}{\theta_u^-}\int_0^{\theta_u^-}\left(1 + \frac{R^-(r,\theta^-)}{a}\right)^{(1-n)} d\theta^-\right] + \left[1 - \left(\frac{\theta_u^-}{\pi}\right)\right]\left[1 - \frac{1}{\theta_u^+}\int_0^{\theta_u^+}\left(1 + \frac{R^+(r,\theta^+)}{a}\right)^{(1-n)} d\theta^+\right], \tag{1}$$

with

$$\theta_u^- = \arcsin\left(\frac{R_1}{r}\right), \tag{2}$$

$$\theta_u^+ = \pi - \theta_u^-, \tag{3}$$

$$R^-(r,\theta^-) = r\cos(\theta^-) - \sqrt{(r\cos(\theta^-))^2 + R_1^2 - r^2}, \tag{4}$$

$$R^+(r,\theta^+) = -r\cos(\theta^+) + \sqrt{(r\cos(\theta^+))^2 + R_2^2 - r^2}, \tag{5}$$

where r is the distance of a molecule from the centre of the co-axial cylinders and R^- the travelling distance limit for a molecule moving towards the inner cylinder surface, for a given zenith angle θ^-. The largest travelling distance R_u^- is achieved for the zenith angle direction θ_u^-, above which the molecule bypasses the cylinder surface and travels into the bulk or towards the outer cylinder surface. The molecule has a travelling distance of R^+ to the outer cylinder surface for a travelling direction of θ^+.

Here, β is the geometry-dependent normalised MFP based on a power-law distribution function and is dependent on the Knudsen number Kn through the mean free path λ and a geometry constraint

R_2/R_1. The Knudsen number is defined as

$$Kn = \frac{\lambda}{R_2 - R_1}. \tag{6}$$

The power-law exponent n acts as a decisive parameter to define the extent of deviation from equilibrium. For larger values of n ($\rightarrow \infty$) the PL distribution function simply reduces to the classical exponential one,[45] i.e., molecules follow Brownian motion rather than Lévy-type flights.[30] For a finite n, the distribution function describes a system deviating from equilibrium. Through MD simulations, Dongari *et al.*[29,31] determined that an n value of 3 in both the slip and transition regimes gave very good results for both isothermal and thermal gas flows in planar and non-planar geometries.[32] Therefore, we use $n = 3$ for all of our PL model results presented in this paper, although we recognise that the value of this parameter should usefully be the subject of future investigations.

B. Shear flow between two parallel plates

The physics of Knudsen layers is best illustrated through a simple set-up of shear flow between two parallel plates. Ansumali *et al.*[18] provided the exact solution to the hierarchy of nonlinear lattice Boltzmann kinetic equations for the stationary planar Couette flow test case. They presented not only the slip velocity results as a function of Knudsen number, but also the shear stress and normal stress difference, which arise due to the non-continuum effects. Other researchers have also carried out studies on planar Couette flow in order to analyse Knudsen layer effects in near-wall regions.[10,19,46]

The flow is assumed to be fully developed, one-dimensional, isothermal, laminar, and steady, with a low Reynolds number (Re) so that inertial effects may be neglected. As $Ma^2 Kn^2$ is assumed to be very small, non-continuum effects which trigger a normal stress difference are also negligible. With these assumptions, the governing equation and the first-order slip boundary condition for planar Couette flow can be given as

$$\frac{\partial}{\partial y}\left(\beta_{\mathrm{PL}} \frac{\partial U}{\partial y}\right) = 0, \tag{7}$$

$$U_{slip} = U_w - C_1 Kn \left(\beta_{\mathrm{PL}} \frac{\partial U}{\partial y}\right)_w, \tag{8}$$

where β_{PL} is the normalised effective mean free path in planar geometries,[29,31] U_w is the wall velocity, and C_1 is the first-order slip velocity coefficient (taken as unity).

The distance between the two parallel plates is H, and they are set at $y = \pm H/2$. The Knudsen number is given by $Kn = \lambda/H$. The upper and lower plates move with a constant velocity $U_w = \pm 50$ m s^{-1}, in opposite directions, and the external acceleration $a_x = a_y = 0$. Energy transfer considerations are not included at this stage, but the plate temperatures are considered to be equal and constant to allow the properties of the gas flow to be determined. Equation (7) is numerically solved for the normalised axial velocity profiles U^* by applying the slip boundary condition (8) at the upper and lower walls (i.e., at $y^* = \pm 0.5$). A second-order slip boundary condition has not been implemented, as the higher order term reduces to zero due to Eq. (7).

In Figure 4, we compare our PL model with the DSMC data, and results of the R13 and R26 equations,[46] in order to illustrate the predictive capabilities of our Navier-Stokes based continuum equations relative to other extended hydrodynamic models. We chose to compare our results with the DSMC data of Gu and Emerson,[46] as their simulations are carried out for a very low Mach number, which is consistent with our assumption of neglecting inertial forces. In the early transition regime, $Kn = 0.25$, the velocity profile predicted by the R13 equations is linear. In the core part of the flow (i.e., outside of the Knudsen layer), all three hydrodynamic models are in agreement with the DSMC data.[46] However, in the region close to the wall, the DSMC results indicate a Knudsen-layer velocity profile, i.e., nonlinear variations. The R13 equations do not follow this behaviour, while the PL model and the R26 equations are in excellent agreement with the DSMC data. At $Kn = 0.5$ and above, i.e., well into the transition regime, the DSMC data clearly show the expected Knudsen-layer velocity profile with substantial velocity slip at the surface due to strong rarefaction effects. The R13

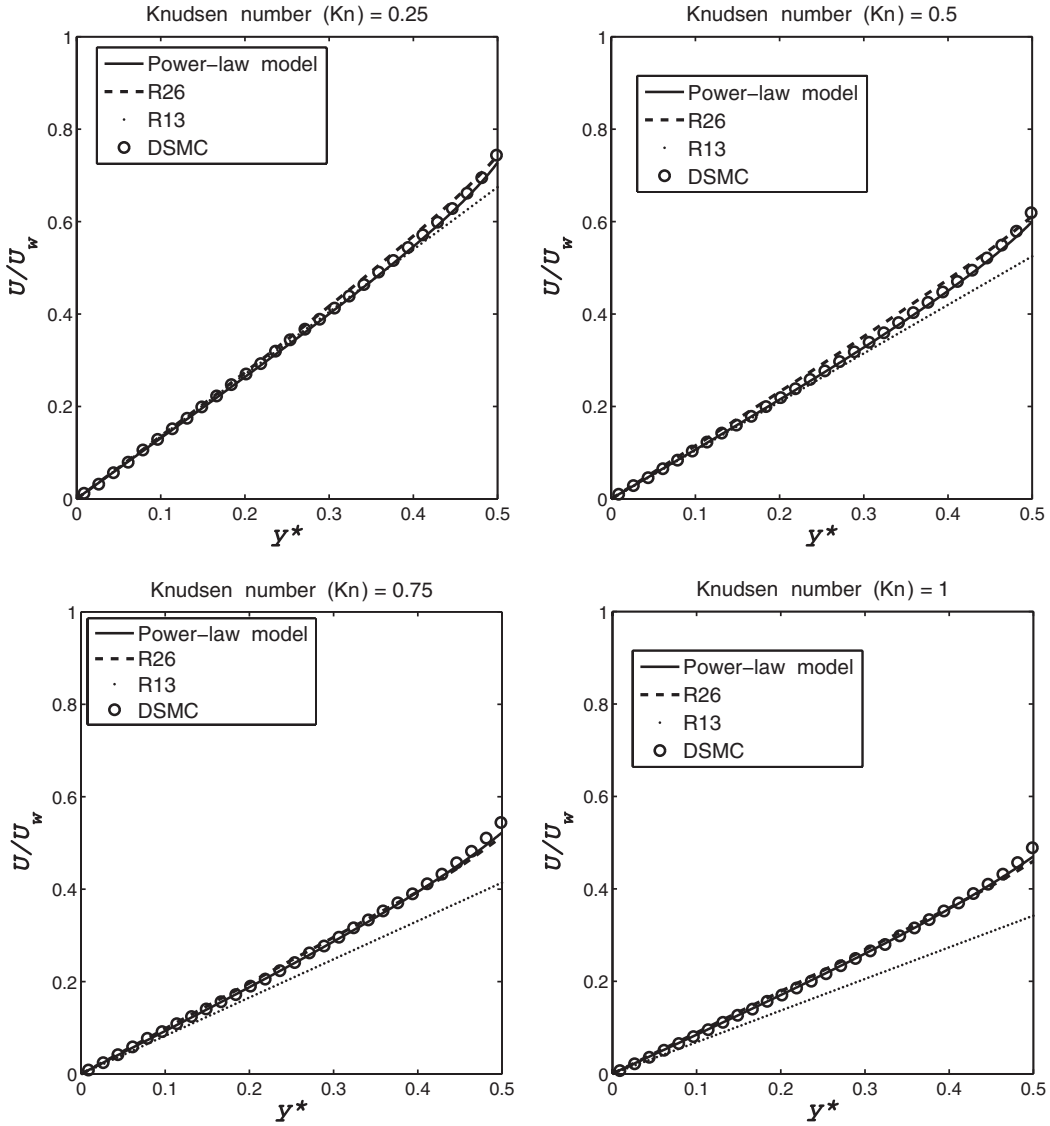

FIG. 4. Normalised half channel velocity profiles for planar Couette flow at various Knudsen numbers. Comparison of our power-law (PL) model results with the DSMC data, and the R26 and R13 moment equations.[46]

equations fail to capture this aspect of the velocity profile, and overpredict the amount of velocity slip. In contrast, the results from the PL model are in very good agreement with both the DSMC data and the R26 equations, and the new model not only predicts the correct velocity slip but also, and more importantly, captures the power-law behaviour of the velocity profile in the Knudsen layer,[47] even up to $Kn = 1.0$.

IV. CYLINDRICAL COUETTE FLOW

A. Governing equations

We consider a rarefied gas confined between two concentric rotating cylinders as shown in Figure 3. The flow is assumed to be fully developed, two-dimensional, isothermal, laminar, and steady, with a low Reynolds number ($0.32 \leq Re \leq 3.22$ for the cases considered) so that inertial effects may be neglected. As Ma^2Kn^2 is assumed to be very small, non-continuum effects which trigger normal stress difference are also negligible. With these assumptions, the governing flow

equation in cylindrical coordinates is

$$\frac{1}{r^2}\frac{d}{dr}\left(r^2\tau_{r\phi}\right) = 0, \tag{9}$$

where r is the radial coordinate, ϕ is the tangential coordinate, and $\tau_{r\phi}$ is the tangential stress, which is defined as

$$\tau_{r\phi} = \mu\left(\frac{du_\phi}{dr} - \frac{u_\phi}{r}\right), \tag{10}$$

where μ is the fluid dynamic viscosity and u_ϕ is the velocity of the fluid in the tangential direction.

From the kinetic theory of gases, the fluid viscosity can be understood in terms of the collisions between gas molecules, and of the free paths of molecules between collisions. The unconfined MFP is then related to the shear viscosity:[48]

$$\mu = \rho\frac{\lambda}{\sqrt{\pi/2RT}}, \tag{11}$$

where ρ is the gas density, R the specific gas constant, and T the gas temperature.

Equation (11) is only valid for flows that are in quasi-equilibrium. Within the Knudsen layer, the flight paths of the gas molecules are affected by the presence of a surface. If the unconfined expression for the MFP, λ, is replaced by our geometry-dependent mean free path for the non-planar case, $\lambda_{\text{eff}} = \lambda\beta$ through Eq. (1), we obtain a non-constant, geometry-dependent, effective viscosity, μ_{eff}, that can then be used to deduce a nonlinear stress/strain-rate relation:

$$\tau_{r\phi} = \underbrace{\mu\beta}_{\mu_{\text{eff}}}\left(\frac{du_\phi}{dr} - \frac{u_\phi}{r}\right). \tag{12}$$

Substituting Eq. (12) into Eq. (9) results in the modified governing equation:

$$\frac{\mu}{r^2}\frac{d}{dr}\left[r^2\beta\left(\frac{du_\phi}{dr} - \frac{u_\phi}{r}\right)\right] = 0. \tag{13}$$

This model needs to be solved in conjunction with the following slip boundary conditions at the inner and outer cylinder surfaces, respectively,

$$u_\phi\,|_{r=R_1} = \omega_1 R_1 + \underbrace{\frac{2-\sigma_1}{\sigma_1}}_{\alpha_1}\lambda\left[\beta\left(\frac{du_\phi}{dr} - \frac{u_\phi}{r}\right)\right]_{r=R_1}, \tag{14}$$

$$u_\phi\,|_{r=R_2} = \omega_2 R_2 - \underbrace{\frac{2-\sigma_2}{\sigma_2}}_{\alpha_2}\lambda\left[\beta\left(\frac{du_\phi}{dr} - \frac{u_\phi}{r}\right)\right]_{r=R_2}, \tag{15}$$

where ω_1 and ω_2 are the angular velocities and σ_1 and σ_2 are the tangential momentum accommodation coefficients of the inner and outer cylinders, respectively.

The solution for the velocity profile can then be obtained as

$$u_\phi(r) = r\left[\omega_1 + \frac{\alpha_1\lambda C}{R_1^3} + G(r)C\right], \tag{16}$$

where

$$G(r) = \int_{R_1}^{r}\frac{dr}{r^3\beta}, \tag{17}$$

$$C = \frac{\omega_2 - \omega_1}{\left[H_1 + \frac{\alpha_1\lambda}{R_1^3} + \frac{\alpha_2\lambda}{R_2^3}\right]}, \tag{18}$$

$$H_1 = \int_{R_1}^{R_2}\frac{dr}{r^3\beta}. \tag{19}$$

When the effects of the Knudsen layer are neglected, i.e., the mean free path has no geometry dependence, then Eq. (16) simply reduces to the velocity profile based on the classical slip solution, as presented in Yuhong *et al.*[5]

The accurate prediction of integral flow parameters in micro-/nano-conduits is important in engineering MEMS devices. Here, the torque exerted on the rotating inner cylinder is given as

$$\Gamma = fAR_1, \tag{20}$$

with

$$f = \left[\mu_{\text{eff}}\left(\frac{du_\phi}{dr} - \frac{u_\phi}{r}\right)\right]_{r=R_1}, \tag{21}$$

$$A = 2\pi R_1 L, \tag{22}$$

where L is the length of the inner cylinder.

When the no-slip boundary condition is applied and the Knudsen layer effects are negligible, the torque expression for flows in the continuum regime is[14]

$$\Gamma_C = \frac{4\pi\mu\omega L}{\left(\frac{1}{R_1^2} - \frac{1}{R_2^2}\right)}. \tag{23}$$

V. RESULTS AND DISCUSSION

Normalised velocity profiles [$U^* = u_\phi/(\omega_1 R_1)$] are presented in Figures 5–11 for various Knudsen numbers and R_2/R_1 values, and different combinations of accommodation coefficients. To highlight the phenomenon of velocity inversion, the outer cylinder is kept stationary ($\omega_2 = 0$) and the inner cylinder is allowed to rotate. For an initial study, the ratio of the radii of the inner and outer cylinders R_2/R_1 is chosen to be 5/3, and the accommodation coefficients are assumed to be equal at the inner and outer surfaces ($\sigma_1 = \sigma_2 = \sigma$). Figure 5(a) presents a comparison between our solution based on the PL effective MFP (Eq. (16)) and the DSMC data. The PL model is in excellent agreement with the simulation data for the $Kn = 0.1$ case, at all σ values. Figure 5(b) presents the results based on the classical governing equation together with the conventional slip boundary conditions, i.e., without considering any Knudsen layer effects (see Yuhong *et al.*[5]), alongside the PL model results. The classical slip model results are in good agreement with the PL, with slight deviations in the near-wall regions. For $Kn = 0.1$, i.e., the end of the slip flow regime, no velocity inversion is predicted by either the simulation data or the theoretical models.

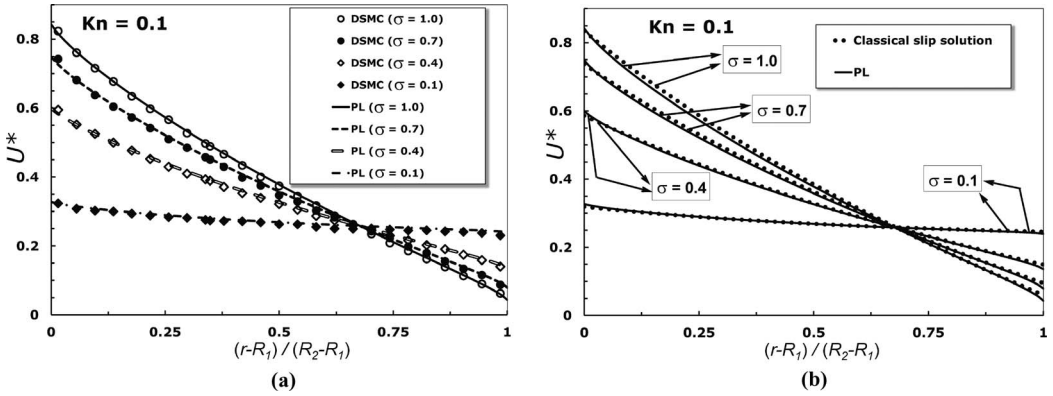

FIG. 5. Variation of the non-dimensional velocity [$U^* = u_\phi/(\omega_1 R_1)$] with normalised radial distance for cylindrical Couette flow with $\sigma_1 = \sigma_2 = \sigma$. Comparison of PL model results against (a) DSMC data and (b) the classical slip solution (Yuhong *et al.*[5]). The results are presented for $Kn = 0.1$ and $R_2/R_1 = 5/3$.

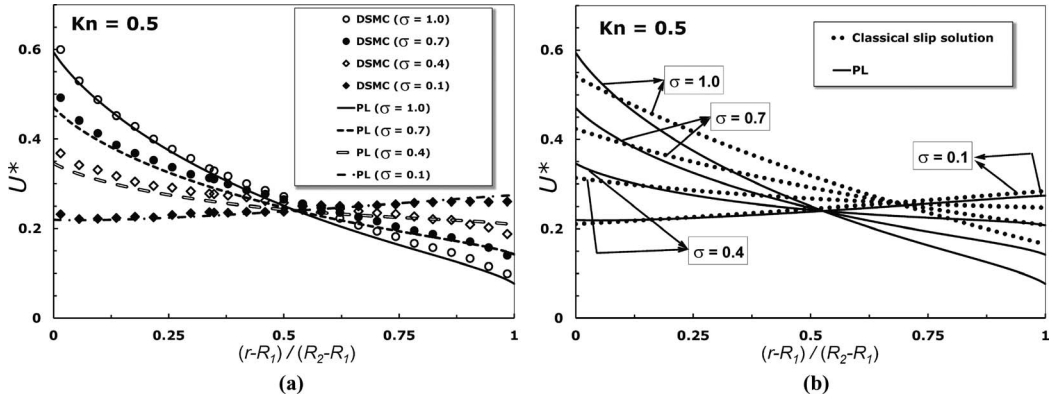

FIG. 6. Variation of the non-dimensional velocity $[U^* = u_\phi/(\omega_1 R_1)]$ with normalised radial distance for cylindrical Couette flow with $\sigma_1 = \sigma_2 = \sigma$. Comparison of PL model results against (a) DSMC data and (b) the classical slip solution.[5] The results are presented for $Kn = 0.5$ and $R_2/R_1 = 5/3$.

Comparisons for the $Kn = 0.5$ case are presented in Figure 6. The PL model is in very good quantitative agreement with the DSMC results for the $\sigma = 1.0$ and 0.7 cases. The results show that the DSMC data and PL formulation follow the same basic trends and predict an inverted velocity profile when the accommodation coefficient is 0.1. However, slight deviations are discernible at the surface of the outer cylinder for the $\sigma = 0.4$ and 0.1 cases. It is interesting to note that, for the specific case of the accommodation coefficients of the inner and outer cylinders having the same value, the family of velocity profiles all pass through a common point that is independent of the value of the accommodation coefficient. This intersection point in the PL profiles is fairly close to the point predicted by the DSMC data, whereas the classical slip solution predicts this point closer to the outer cylinder, as shown in Figure 6(b). The classical slip solution does not account for any variation in MFP and hence fails to capture nonlinear effects associated with the Knudsen layers at the inner and outer cylinders; it underpredicts the slip velocity at the inner cylinder and overpredicts at the outer one, i.e., accounting for larger slip effects. The discrepancies are greatest at $\sigma = 1.0$ and decrease as σ is reduced. At very low values of σ, the PL model and classical slip solutions are identical and yield the same solid body rotation solution as $\sigma \to 0$.

Figure 7 shows velocity profiles for the $Kn = 1$ case, and deviations between the PL model and DSMC data are discernible in the near-wall regions at both the inner and outer cylinders, for all σ values. The PL model underpredicts the slip velocities at the inner cylinder for all σ values; however, at the outer cylinder it overpredicts for $\sigma = 0.1$, 0.4, and 0.7, and slightly underpredicts

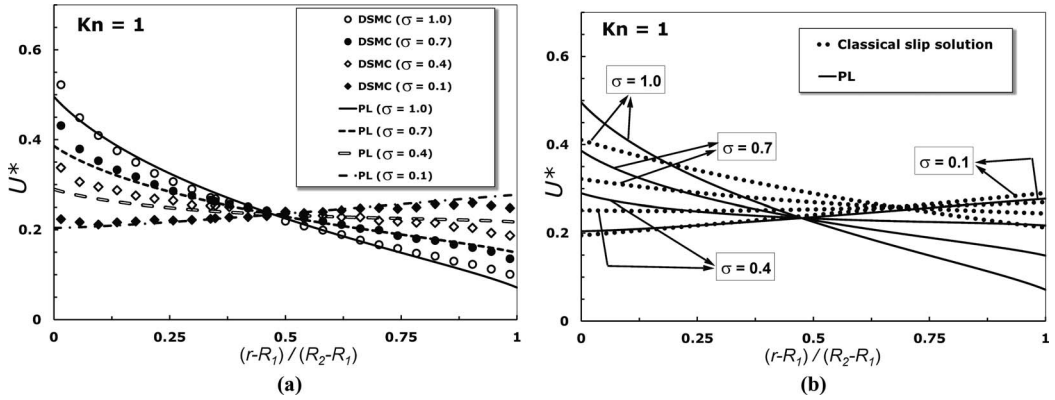

FIG. 7. Variation of the non-dimensional velocity $[U^* = u_\phi/(\omega_1 R_1)]$ with normalised radial distance for cylindrical Couette flow with $\sigma_1 = \sigma_2 = \sigma$. Comparison of PL model results against (a) DSMC data and (b) the classical slip solution.[5] The results are presented for $Kn = 1.0$ and $R_2/R_1 = 5/3$.

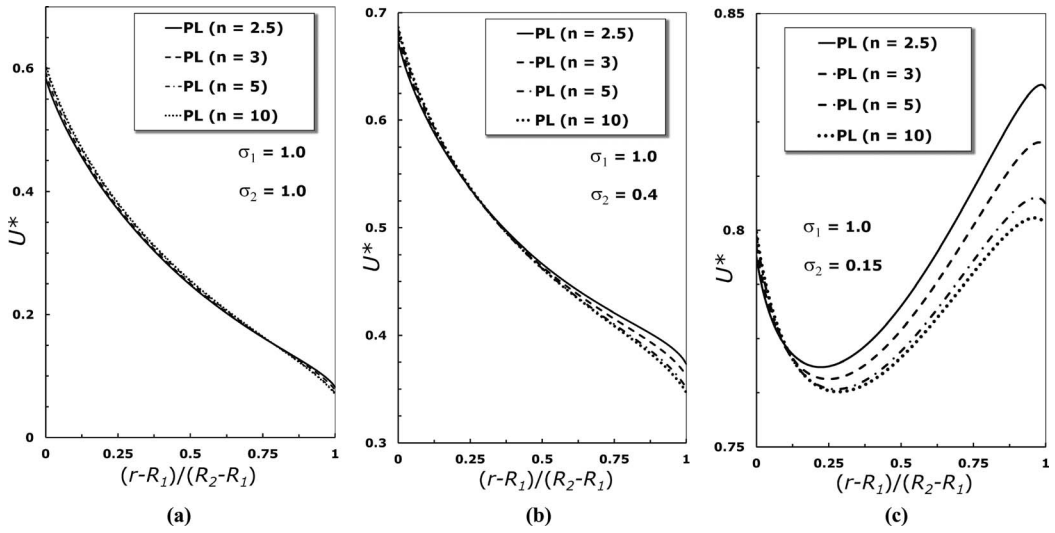

FIG. 8. Effect of the power-law (PL) exponent n on the cylindrical Couette flow velocity profiles. Variation of the non-dimensional velocity $[U^* = u_\phi/(\omega_1 R_1)]$ with normalised radial distance for $\sigma_1 = 1.0$ and (a) $\sigma_2 = 1.0$, (b) $\sigma_2 = 0.4$, and (c) $\sigma_2 = 0.15$, for $Kn = 0.5$ and $R_2/R_1 = 5/3$.

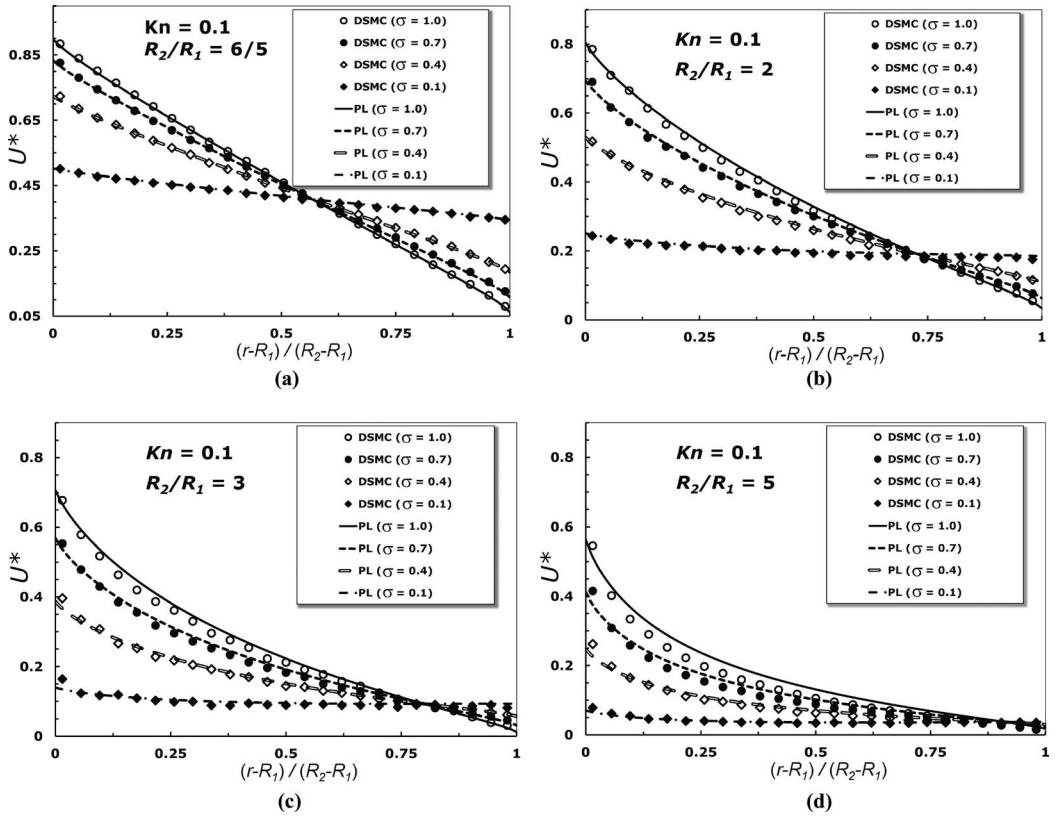

FIG. 9. Variation of the non-dimensional velocity $[U^* = u_\phi/(\omega_1 R_1)]$ with normalised radial distance for cylindrical Couette flow with $\sigma_1 = \sigma_2 = \sigma$. Comparison of PL model results against DSMC data. The results are presented for $Kn = 0.1$ and $R_2/R_1 = 6/5$ (top left), 2 (top right), 3 (bottom left), and 5 (bottom right).

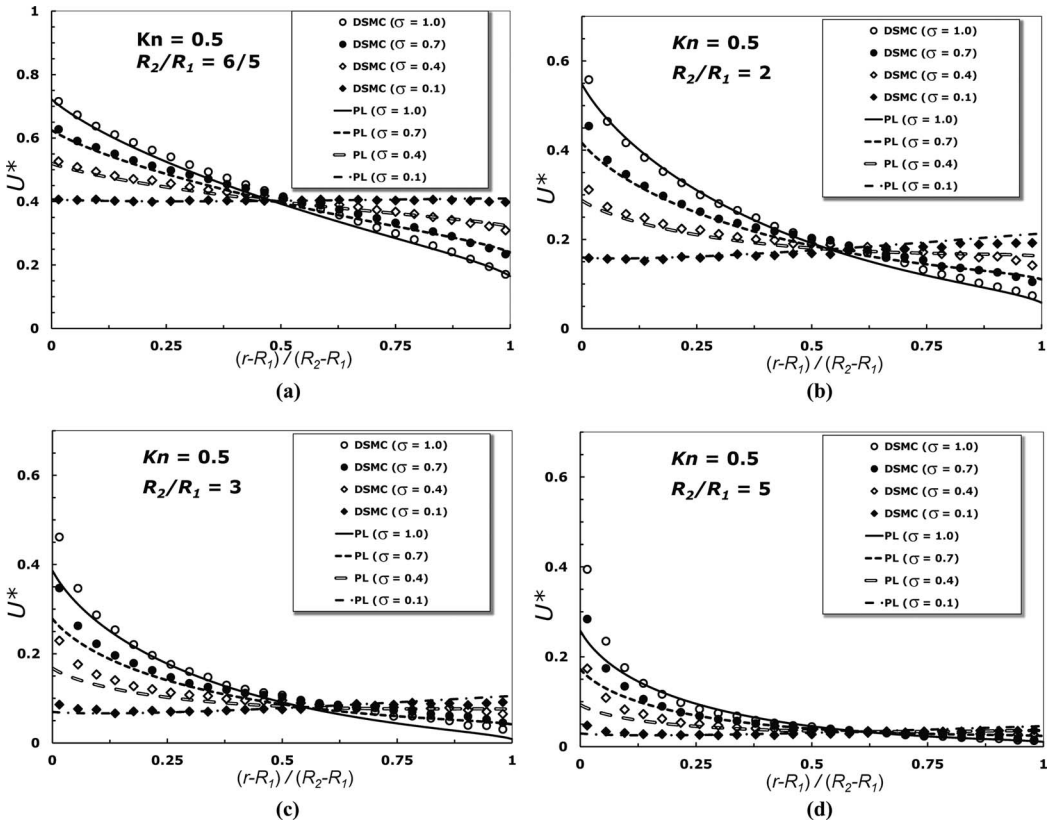

FIG. 10. Variation of the non-dimensional velocity [$U^* = u_\phi/(\omega_1 R_1)$] with normalised radial distance for cylindrical Couette flow with $\sigma_1 = \sigma_2 = \sigma$. Comparison of PL model results against DSMC data. The results are presented for $Kn = 0.5$ and $R_2/R_1 = 6/5$ (top left), 2 (top right), 3 (bottom left), and 5 (bottom right).

for $\sigma = 1$. The classical slip model comparisons with the PL model are qualitatively similar to the $Kn = 0.5$ case. The intersection point of the family of velocity profiles, for both the DSMC data and the PL model, moves towards the inner cylinder as Kn increases. However, for the classical slip model, the intersection point is found to stay at about the same location (approximately 0.7 on the abscissa) for all Kn cases.

As mentioned earlier, the value of the power-law exponent has been fixed to $n = 3$ for all the reported results so far. Figure 8 demonstrates the effect of the value of n on the structure of the velocity profile in the Knudsen layer, for $\sigma_1 = 1.0$ and (a) $\sigma_2 = 1.0$, (b) $\sigma_2 = 0.4$, and (c) $\sigma_2 = 0.15$. The velocity profiles are almost unaffected by the value of n at high values of the accommodation coefficients ($\sigma_2 = 1.0$) across the entire annular clearance. For small accommodation coefficients ($\sigma_2 = 0.4$ and 0.15), the velocity profiles are shown to depend on the value of n, and the sensitivity to this increases towards the outer cylinder. However, the maximum deviation is limited to only around 3%–4%, and this is obtained with n varying from 2.5 to 10. As mentioned in the paper, previous MD results indicate that the value of n is around 3, and so velocity profiles may not be too sensitive to small variations in n.

To check the sensitivity of curvature effects on the velocity profiles, we now present results for $R_2/R_1 = 6/5$, 2, 3, and 5 cases, and at $Kn = 0.1$, 0.5, and 1. The radii ratio is varied by fixing R_1 and increasing R_2, and Kn is set by modifying the gas density. The Reynolds number (Re) is the same for different geometric configurations for a given Kn, as Ma is kept constant.

Figure 9 demonstrates the velocity profiles for the $Kn = 0.1$ case, at different R_2/R_1 values. For each R_2/R_1 value, the PL model results are compared with DSMC data for $\sigma = 0.1$, 0.4, 0.7, and 1. For lower R_2/R_1 values (6/5 and 2), the PL model is in excellent agreement with simulation data in the whole of the annular gap. However, with an increase in R_2/R_1, deviations are noticed in

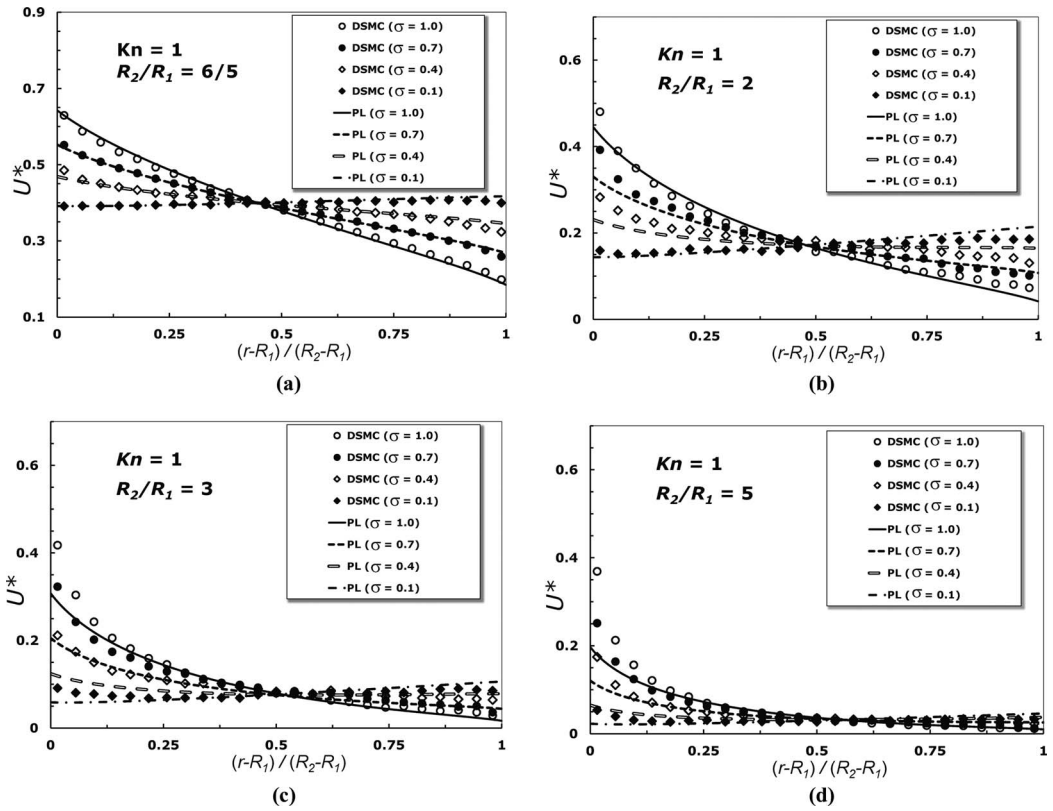

FIG. 11. Variation of the non-dimensional velocity [$U^* = u_\phi/(\omega_1 R_1)$] with normalised radial distance for cylindrical Couette flow with $\sigma_1 = \sigma_2 = \sigma$. Comparison of PL model results against DSMC data. The results are presented for $Kn = 1$ and $R_2/R_1 = 6/5$ (top left), 2 (top right), 3 (bottom left), and 5 (bottom right).

the near-wall region at the inner cylinder. Here the PL model slightly underpredicts the wall-slip velocities for the $R_2/R_1 = 3$ and 5 cases, although at the outer cylinder velocities are accurately predicted. The profiles intersection point moves towards the outer cylinder with an increase in R_2/R_1.

Slip velocities decrease at both the inner and the outer cylinders with an increase in R_2/R_1. When the size of the inner cylinder is relatively reduced in comparison with the outer one, relatively larger and smaller slip effects are noticed, at the inner and outer cylinders, respectively. This may be due to relatively fewer molecules interacting with the inner cylinder, compared to the outer one. On the other hand, for the $R_2/R_1 = 6/5$ case, no velocity inversion is observed at $\sigma = 0.1$; however, partially inverted velocity profiles are predicted in cases with higher values of R_2/R_1. For partial inversions, the gradient of the velocity profile has to be zero at some position in the annular gap, and this point moves towards the inner cylinder with an increase in R_2/R_1.

Similar comparisons are carried out for $Kn = 0.5$ and 1 cases, and are shown in Figures 10 and 11. For the $R_2/R_1 = 6/5$ case, the PL model is in excellent agreement with DSMC data at both $Kn = 0.5$ and 1. Deviations are noticed as R_2/R_1 increases, becoming quite significant for the $R_2/R_1 = 5$ case, especially in the near-wall region of the inner cylinder. Similar to the $Kn = 0.1$ case, the slip velocities at the inner cylinder decrease significantly with an increase in R_2/R_1. For the $Kn = 0.5$ and $\sigma = 1$ case, with an increase in R_2/R_1, the slip velocities at the inner cylinder predicted by DSMC vary approximately from 0.73 to 0.4, whereas for the PL model from 0.72 to 0.25. For the $Kn = 1$ and $\sigma = 1$ case, they vary from 0.7 to 0.38, and from 0.68 to 0.2, for the DSMC and PL model, respectively. This conveys that deviations between the PL model and our DSMC data approximately vary from 1% to 38% with an increase in R_2/R_1 from 6/5 to 5, for the $Kn = 0.5$ and $\sigma = 1$ case. They vary from 2% to 47% with an increase in R_2/R_1 from 6/5 to 5, for the $Kn = 1$ and $\sigma = 1$ case. Deviations decrease with decrease in σ, and hence the above mentioned deviations of the PL model illustrate the maximum ones. With an increase in curvature effects, deviations are

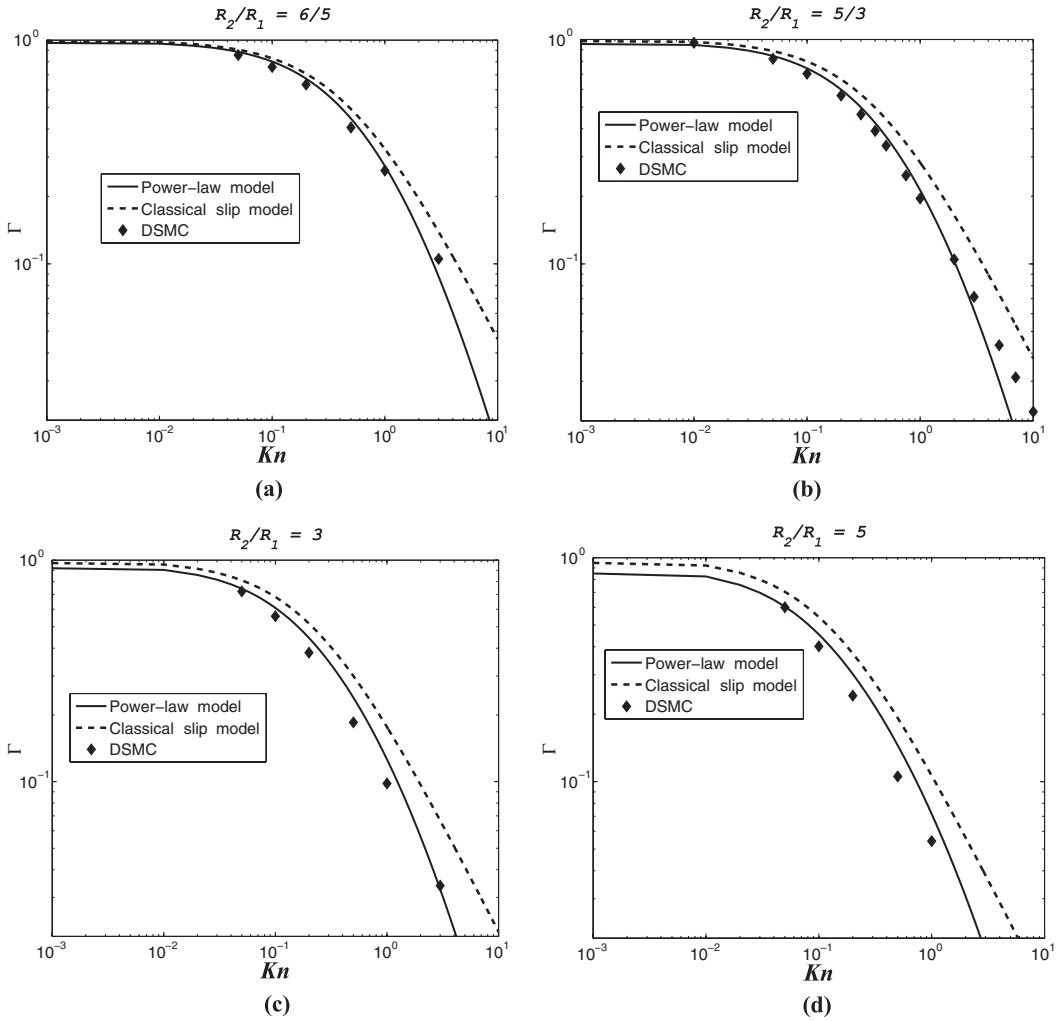

FIG. 12. Variation of normalised torque Γ exerted on the rotating inner cylinder with Knudsen number (Kn). Our DSMC data are compared with both the slip and the PL models. The data are obtained for a specific case, where the accommodation coefficients of both the inner and outer cylinders are unity ($\sigma_1 = \sigma_2 = 1$) and $R_2/R_1 = 6/5$ (top left), 5/3 (top right), 3 (bottom left), and 5 (bottom right).

significant in the transition regime, which suggests that the simple power-law free path distribution function has limitations and it needs to be revisited for larger curvature geometries.

The position of the profile intersection point is relatively insensitive to a change in R_2/R_1 for the $Kn = 0.5$ and 1 cases, when compared with the $Kn = 0.1$ one. On the other hand, for the $R_2/R_1 = 6/5$ case, complete velocity inversion is observed at $\sigma = 0.1$, and only partially inverted velocity profiles are predicted for higher values of R_2/R_1, at $\sigma = 0.1$. For the $Kn = 0.5$ and 1 cases, the position where the gradient of the velocity profile becomes zero moves away from the inner cylinder with an increase in R_2/R_1. These findings are in contrast with the velocity profiles for the $Kn = 0.1$ case, see Figure 9.

Figure 12 presents the variation of the normalised torque (Γ) exerted on the rotating inner cylinder with Knudsen number (Kn), and our DSMC data are compared with the slip and PL models. The data are obtained for a specific case, where the accommodation coefficients of both the inner and the outer cylinders are unity ($\sigma_1 = \sigma_2 = 1$), and for $R_2/R_1 = 6/5$, 5/3, 3, and 5. Torque values are normalised by the continuum-fluid values of the torque (Γ_C), see Eq. (23). The PL model is in good agreement with the DSMC data up to $Kn \sim 2$ for $R_2/R_1 = 6/5$ and 5/3 (i.e., cases with lower curvature). The classical slip model, however, shows substantial

deviations beyond $Kn \sim 0.2$. For cases with larger curvature ($R_2/R_1 = 3$ and 5), the PL model also exhibits deviations from $Kn \sim 0.2$ onwards, although these are limited to 10%–15% up to $Kn = 1$. The classical slip model predicts significant deviations even within the slip flow regime ($Kn \sim 0.05$), which conveys that non-equilibrium effects are more pronounced for larger curvature test cases.

VI. CONCLUSIONS

The non-equilibrium flow physics of isothermal rarefied gases interacting with non-planar surfaces in cylindrical Couette flow has been described using detailed DSMC simulations for different Knudsen numbers, and a variety of accommodation coefficient values and outer-to-inner radius ratios. Simulation data have been compared with both the classical slip theory and our new PL wall scaling model, and both rarefaction and curvature effects on flow properties have been rigorously explored.

Velocity profile comparisons for $Kn = 0.1$, 0.5, and 1, at $R_2/R_1 = 5/3$, highlight the known fact that while the classical slip model is valid in the slip flow regime, it exhibits significant deviations in the transition regime. However, our PL wall scaling model predictions are in very good agreement up to $Kn \sim 1$, with only slight deviations in the near-wall region at the inner cylinder. The simulation data and the PL model also predict partially inverted velocity profiles for moderate σ values, whereas the classical slip model does not capture this phenomenon. The classical slip theory significantly underpredicts the velocity profile at the inner cylinder and overpredicts it at the outer cylinder, and velocity inversion is also predicted at the incorrect σ values (see Figures 6(b) and 7(b)). Our torque investigations indicate that classical slip flow theory may also not be accurate enough even in the slip flow regime for larger curvature test cases.

The DSMC data of velocity profiles for larger R_2/R_1 values illuminate the limitations of the PL wall scaling model in the transition regime. With an increase in the R_2/R_1 value and for $Kn \geq 0.5$, the PL model significantly underpredicts the velocity in the near-wall region of the inner cylinder, but does obtain fair comparison in the near-wall region of the outer one. This shows that the non-equilibrium effects in the near-wall region are not merely dependent on Kn, but that they are also influenced by curvature, since deviations between the DSMC data and PL model are more pronounced for larger R_2/R_1 values. These findings are consistent with our DSMC torque measurements, where the deviations from continuum theory are higher for larger R_2/R_1 (different geometric configurations), for a given Kn and Ma (i.e., a fixed Reynolds number).

Although the predictive capabilities of the PL model are fair for torque comparisons up to the transition regime, the model fails to capture some of nonlinear trends associated with the Knudsen layers at the inner cylinder, as shown in Figures 10 and 11 for $R_2/R_1 = 3$ and 5. Hence, torque and velocity profile comparisons together convey that mere prediction of integral flow parameters does not guarantee the complete accuracy of any theoretical model, and it is important to demonstrate that the field variables are also in agreement with other accurate simulation data.

The major advantage of our new PL model is that it can be easily implemented in conventional computational fluid dynamics (CFD) solvers in order to produce substantially better results in Knudsen layers when compared to the classical slip model. This is very pertinent from the point of view of simulation of fluid flows in arbitrary geometries, as the DSMC method is computationally intensive. In our comparisons with DSMC data in the current paper we used the PL exponent $n = 3$, as in previous planar test cases,[29,31] and $n = 3$ may be applicable in non-planar test cases with lower curvature. However, the current results may motivate future work into understanding the Knudsen layers in arbitrary geometries, including:

(i) rigorous molecular dynamics simulations of rarefied gases confined in arbitrary geometries and subjected to a range of complex flow conditions, for establishing properly and generally the value of n for non-planar cases;
(ii) whether Lévy free flights are an appropriate model for molecules of rarefied gases in non-planar geometries, or whether an alternative form of distribution function is necessary;

(iii) revisiting the classical slip and jump boundary conditions, where were originally derived assuming constant MFP in Knudsen layers, and using geometry-dependent effective MFP models instead.

ACKNOWLEDGMENTS

The research leading to these results has received funding from the European Community's Seventh Framework Programme FP7/2007-2013 under grant agreement ITN GASMEMS (Grant Agreement No. 215504). The author C.W. gratefully acknowledges funding from the James Weir Foundation. The author J.M.R. gratefully acknowledges funding through EPSRC Programme Grant EP/I011927/1. Our calculations were performed on the 1100 core HPC Facility of the Faculty of Engineering at the University of Strathclyde. The authors thank the reviewers for their useful comments.

[1] H. Schlichting and K. Gersten, *Boundary Layer Theory* (Springer-Verlag, Berlin, 2000).
[2] D. Einzel, P. Panzer, and M. Liu, "Boundary condition for fluid flow: Curved or rough surfaces," Phys. Rev. Lett. **64**, 2269–2272 (1990).
[3] K. W. Tibbs, F. Baras, and A. L. Garcia, "Anomalous flow profile due to the curvature effect on slip length," Phys. Rev. E **56**, 2282–2283 (1997).
[4] K. Aoki, H. Yoshida, T. Nakanishi, and A. L. Garcia, "Inverted velocity profile in the cylindrical Couette flow of a rarefied gas," Phys. Rev. E **68**, 016302 (2003).
[5] S. Yuhong, R. W. Barber, and D. R. Emerson, "Inverted velocity profiles in rarefied cylindrical Couette gas flow and the impact of the accommodation coefficient," Phys. Fluids **17**(4), 047102 (2005).
[6] Z. Guo, B. Shi, and C. Zheng, "Velocity inversion of micro cylindrical Couette flow: A lattice Boltzmann study," Comput. Math. Appl. **61**(12), 3519–3527 (2011).
[7] D. A. Lockerby, J. M. Reese, D. R. Emerson, and R. W. Barber, "Velocity boundary condition at solid walls in rarefied gas calculations," Phys. Rev. E **70**, 017303 (2004).
[8] R. S. Myong, J. M. Reese, R. W. Barber, and D. R. Emerson, "Velocity slip in microscale cylindrical Couette flow: The Langmuir model," Phys. Fluids **17**(8), 087105 (2005).
[9] P. Taheri and H. Struchtrup, "Effects of rarefaction in microflows between coaxial cylinders," Phys. Rev. E **80**, 066317 (2009).
[10] P. Taheri, M. Torrilhon, and H. Struchtrup, "Couette and Poiseuille microflows: Analytical solutions for regularized 13-moment equations," Phys. Fluids **21**(1), 017102 (2009).
[11] W. P. Yudistiawan, S. Ansumali, and I. V. Karlin, "Hydrodynamics beyond Navier-Stokes: The slip flow model," Phys. Rev. E **78**, 016705 (2008).
[12] D. A. Lockerby and J. M. Reese, "High-resolution Burnett simulations of micro Couette flow and heat transfer," J. Comput. Phys. **188**(2), 333–347 (2003).
[13] D. R. Emerson, X. J. Gu, S. K. Stefanov, S. Yuhong, and R. W. Barber, "Nonplanar oscillatory shear flow: From the continuum to the free-molecular regime," Phys. Fluids **19**(10), 107105 (2007).
[14] A. Agrawal and S. V. Prabhu, "Deduction of slip coefficient in slip and transition regimes from existing cylindrical Couette flow data," Exp. Therm. Fluid Sci. **32**(4), 991–996 (2008).
[15] A. Agrawal and S. V. Prabhu, "Survey on measurement of tangential momentum accommodation coefficient," J. Vac. Sci. Technol. A **26**, 634–645 (2008).
[16] D. A. Lockerby, J. M. Reese, and M. A. Gallis, "The usefulness of higher-order constitutive relations for describing the Knudsen layer," Phys. Fluids **17**(10), 100609 (2005).
[17] S. Chapman and T. G. Cowling, *Mathematical Theory of Non-Uniform Gases* (Cambridge University Press, Cambridge, 1970).
[18] S. Ansumali, I. V. Karlin, S. Arcidiacono, A. Abbas, and N. I. Prasianakis, "Hydrodynamics beyond Navier-Stokes: Exact solution to the lattice Boltzmann hierarchy," Phys. Rev. Lett. **98**, 124502 (2007).
[19] W. P. Yudistiawan, S. K. Kwak, D. V. Patil, and S. Ansumali, "Higher-order Galilean-invariant lattice Boltzmann model for microflows: Single-component gas," Phys. Rev. E **82**, 046701 (2010).
[20] C. Cercignani, *The Boltzmann Equation and its Applications* (Springer, New York, 1988).
[21] Y. Sone, *Kinetic Theory and Fluid Dynamics* (Birkhauser, Boston, 2002).
[22] P. Bahukudumbi, J. H. Park, and A. Beskok, "A unified engineering model for steady and unsteady shear-driven gas microflows," Microscale Thermophys. Eng. **7**, 291–315 (2003).
[23] G. Karniadakis, A. Beskok, and N. Aluru, *Microflows and Nanoflows: Fundamentals and Simulation* (Springer, 2005).
[24] N. Dongari, A. Sharma, and F. Durst, "Pressure-driven diffusive gas flows in micro-channels: From the Knudsen to the continuum regimes," Microfluid. Nanofluid. **6**(5), 679–692 (2009).
[25] Y. H. Zhang, X. J. Gu, R. W. Barber, and D. R. Emerson, "Capturing Knudsen layer phenomena using a lattice Boltzmann model," Phys. Rev. E **74**, 046704 (2006).
[26] C. R. Lilley and J. E. Sader, "Velocity profile in the Knudsen layer according to the Boltzmann equation," Proc. R. Soc. London, Ser. A **464**, 2015–2035 (2008).
[27] D. A. Lockerby and J. M. Reese, "On the modelling of isothermal gas flows at the microscale," J. Fluid Mech. **604**, 235–261 (2008).

[28] N. Dongari, F. Durst, and S. Chakraborty, "Predicting microscale gas flows and rarefaction effects through extended Navier-Stokes-Fourier equations from phoretic transport considerations," Microfluid. Nanofluid. **9**, 831–846 (2010).
[29] N. Dongari, Y. H. Zhang, and J. M. Reese, "Molecular free path distribution in rarefied gases," J. Phys. D **44**, 125502 (2011).
[30] M. F. Shlesinger, J. Klafter, and G. Zumofen, "Above, below and beyond Brownian motion," Am. J. Phys. **67**(12), 1253–1259 (1999).
[31] N. Dongari, Y. H. Zhang, and J. M. Reese, "Modeling of Knudsen layer effects in micro/nanoscale gas flows," J. Fluids Eng. **133**(7), 071101 (2011).
[32] N. Dongari, R. W. Barber, D. R. Emerson, S. K. Stefanov, Y. H. Zhang, and J. M. Reese, "The effect of Knudsen layers on rarefied cylindrical Couette gas flows," Microfluid. Nanofluid. **14**, 31–43 (2013); See also "Erratum to: The effect of Knudsen layers on rarefied cylindrical Couette gas flows," Microfluid Nanofluid **14**, 905–906 (2013).
[33] D. W. Stops, "The mean free path of gas molecules in the transition regime," J. Phys. D **3**, 685–696 (1970).
[34] E. J. Arlemark, S. K. Dadzie, and J. M. Reese, "An extension to the Navier-Stokes equations to incorporate gas molecular collisions with boundaries," J. Heat Transfer **132**(4), 041006 (2010).
[35] G. A. Bird, *Molecular Gas Dynamics and the Direct Simulation of Gas Flows* (Oxford University Press, New York, 1994).
[36] D. C. Rapaport, *The Art of Molecular Dynamics Simulation* (Cambridge University Press, Cambridge, 2004).
[37] S. Kim, "Slip velocity and velocity inversion in a cylindrical Couette flow," Phys. Rev. E **79**, 036312 (2009).
[38] Y. Jung, "Velocity inversion in nanochannel flow," Phys. Rev. E **75**, 051203 (2007).
[39] A. R. Kuhlthau, "Air friction on rapidly moving surfaces," J. Appl. Phys. **20**(2), 217–223 (1949).
[40] OpenFOAM Foundation, 2013, see http://www.openfoam.org/.
[41] T. J. Scanlon, E. Roohi, C. White, M. Darbandi, and J. M. Reese, "An open source, parallel DSMC code for rarefied gas flows in arbitrary geometries," Comput. Fluids **39**(10), 2078–2089 (2010).
[42] E. Arlemark, G. Markelov, and S. Nedea, "Rebuilding of Rothe's nozzle measurements with OpenFOAM software," J. Phys.: Conf. Ser. **362**, 012040 (2012).
[43] G. A. Bird, "Definition of mean free path for real gases," Phys. Fluids **26**(11), 3222–3223 (1983).
[44] N. Dongari, R. W. Barber, D. R. Emerson, Y. H. Zhang, and J. M. Reese, "Velocity inversion in cylindrical Couette gas flows," J. Phys.: Conf. Ser. **362**, 012009 (2012).
[45] E. Kennard, *Kinetic Theory of Gases* (McGraw-Hill, London, 1938).
[46] X. J. Gu and D. R. Emerson, "A high-order moment approach for capturing non-equilibrium phenomena in the transition regime," J. Fluid Mech. **636**, 177–226 (2009).
[47] C. R. Lilley and J. E. Sader, "Velocity gradient singularity and structure of the velocity profile in the Knudsen layer according to the Boltzmann equation," Phys. Rev. E **76**, 026315 (2007).
[48] C. Cercignani, *Mathematical Methods in Kinetic Theory* (Plenum Press, New York, 1990).